

CHORUS

This is the accepted manuscript made available via CHORUS. The article has been published as:

Strong dependence of photoionization time delay on energy and angle in the neighborhood of Fano resonances

Sourav Banerjee, Pranawa C. Deshmukh, Valeriy K. Dolmatov, Steven T. Manson, and Anatoli S. Kheifets

Phys. Rev. A **99**, 013416 — Published 14 January 2019

DOI: [10.1103/PhysRevA.99.013416](https://doi.org/10.1103/PhysRevA.99.013416)

Dramatic dependence of photoionization time delay on energy and angle in the neighbourhood of Fano resonances

Sourav Banerjee,¹ Pranawa C. Deshmukh,² Valeriy K. Dolmatov,³ Steven T. Manson,⁴ and Anatoli S. Kheifets⁵

¹ *Department of Physics, Indian Institute Technology Madras, Chennai 600036, India*

² *Department of Physics, Indian Institute of Technology Tirupati, Tirupati, 517 506, India*

³ *Department of Physics and Earth Science, University of Northern Alabama, Florence, AL 35632, USA*

⁴ *Department of Physics and Astronomy, Georgia State University, Atlanta, 30303, USA*

⁵ *Research School of Physics and Engineering, The Australian National University, Canberra ACT 2601, Australia*

(Dated: December 14, 2018)

We uncover dramatic variations of the Wigner photoemission time delay with energy and angle in the vicinity of a Fano resonance with the time delay taking opposite signs at different angles at the same energy as well as at the opposite sides of the resonance at the same angle. These variations are illustrated by choosing the Ne $2s \rightarrow 3p$ autoionizing state as a case study. Moreover, we demonstrate the existence of strikingly significant changes in time delay due to relativistic effects despite Ne being a low- Z atom. This finding shows the possibility for utilizing time delay chronoscopy as a new route towards experimental probing of relativistic interactions and the phases of individual transition matrix elements upon atomic photoionization of low- Z atoms. Finally, we develop a practical parameterization to model and explain the angle and energy variation of the autoionizing resonance time delay in the non-relativistic limit.

PACS numbers: 32.80.Rm, 32.80.Fb, 42.50.Hz

I. INTRODUCTION

Bound states in the continuum (Fano resonances) are omnipresent in nature and their studies remain at the forefront of contemporary physics across various disciplines [1, 2]. With the recent development of ultrashort laser pulses, dynamics of Fano resonances can be studied in real time [3]. One of convenient characterization of this dynamic is the wave packet group delay introduced by Wigner, Eisenbud and Smith [4–6], Wigner time delay (WTD). In laser induced photoionization, it is an important indicator of electron motion on the attosecond time scale. It is expressed as the energy derivative of the phase of the transition matrix element. This phase is otherwise difficult to access, in contrast to the magnitude of the transition matrix which is accessible through the measurable cross sections and transition rates. Thus, determining the WTD is an important step towards a complete characterization of photoemission process. Research in this area was stimulated by two pioneering laboratory studies dealing with photoemission of Ne [7] and Ar [8]. It has subsequently become a subject of intense experimental and theoretical scrutiny. An early review can be found in [9]. Later works are represented by [10–24]. Most of these investigations have involved nonresonant photoemission. A few studies, however, focused on photoionization in the region of Fano resonances [14, 15, 20–23] where the phase, and thus the time delay, changes rapidly over a small energy range.

In the present work, to understand the full extent of this phenomenology, we look at the energy and angle dependence of the WTD in detail to provide a road map for future laboratory investigation. The case of the $2s \rightarrow 3p$ autoionizing resonance in Ne was chosen because: Ne is a noble gas and easily dealt with experimentally; the res-

onance is in an energy region accessible to experimental capabilities; cross section calculations for this resonance, using the same methodology as the present study, have shown excellent agreement with experiment [25], thereby suggesting that the present results should be accurate. Although Ne is a low- Z atom, we employ a fully relativistic formulation based on the Dirac Equation, thus elucidating the role of the relativistic effects.

The present study highlights the following important aspects of the resonant WTD: (i) A strong angular dependence which varies dramatically with the photoemission angle relative to the polarization of light, so strong that it results in sign reversal of the WTD under certain conditions. (ii) The sensitivity of the angular distribution to relativistic effects, even at such a low Z so that the WTD chronoscopy might be a sensitive probe of relativistic interactions. (iii) The possibility of measuring the WTD for individual amplitudes using spin-resolved time-delay chronoscopy.

II. METHODOLOGY

The relativistic formalism of the angular dependent WTD is presented in [26]. Briefly, the electric dipole transition amplitude from an initial state a , ($l j m$), to the final states \bar{a} , ($\bar{l} \bar{j} \bar{m}$), for linearly polarized photons in the \hat{z} direction is, to within an overall real multiplicative factor,

$$T_{10}^{(1\nu)} = \sum_{\bar{\kappa}\bar{m}} (\chi_{\nu}^{\dagger} \Omega_{\bar{\kappa}\bar{m}}(\hat{p})) (-1)^{\bar{j}-\bar{m}} \begin{pmatrix} \bar{j} & 1 & j \\ -\bar{m} & 0 & m \end{pmatrix} \times i^{1-\bar{l}} e^{i\delta_{\bar{\kappa}}} \langle \bar{a} || Q_1^{(1)} || a \rangle (-1)^{\bar{j}+j+1} \quad (1)$$

Here \hat{p} is the photoelectron momentum direction, $\delta_{\bar{\kappa}}$ is the phase of the continuum wave with $\bar{\kappa} = \mp(\bar{j} + \frac{1}{2})$ for $\bar{j} = (\bar{l} \pm \frac{1}{2})$, and the spherical spinor is defined as

$$\Omega_{\kappa m}(\hat{n}) = \sum_{\nu=\pm 1/2} C_{l, m-\nu, 1/2\nu}^{jm} Y_{l m-\nu}(\hat{n}) \chi_{\nu}. \quad (2)$$

Here χ_{ν} is a two-component spinor and C is a Clebsch-Gordan coefficient. We combine the reduced electric dipole matrix element $\langle \bar{a} \| Q_1^{(1)} \| a \rangle$ defined in [26] with the phase factors and introduce

$$D_{l\bar{j} \rightarrow \bar{l}\bar{j}} = i^{1-\bar{l}} e^{i\delta_{\bar{\kappa}}} \langle \bar{a} \| Q_1^{(1)} \| a \rangle, \quad (3)$$

which absorbs all of the complex part of the amplitude except for the spherical harmonics.

Present study deals with the photoionization from the outer p-subshell of neon. Transition amplitudes for the six possible transitions from the spin orbit split np states are tabulated in [26]; the two amplitudes for the $2p_{1/2}$ initial state are:

$$[T_{10}^{1+}]_{2p_{1/2}}^{m=\frac{1}{2}} = \frac{Y_{20}}{\sqrt{15}} D_{2p_{1/2} \rightarrow \epsilon d_{3/2}} + \frac{Y_{00}}{\sqrt{6}} D_{2p_{1/2} \rightarrow \epsilon s_{1/2}} \quad (4)$$

$$[T_{10}^{1-}]_{2p_{1/2}}^{m=\frac{1}{2}} = -\frac{Y_{21}}{\sqrt{10}} D_{2p_{1/2} \rightarrow \epsilon d_{3/2}} \quad (5)$$

These expressions are invariant to the simultaneous sign inversion of the spin and angular momentum projections. Each amplitude is associated with its own WTD defined as

$$\tau_{2p_j}^{\nu m} = \frac{d\eta}{dE}, \quad \eta = \tan^{-1} \left\{ \frac{\text{Im}[T_{10}^{1\nu}]_{2p_j}^m}{\text{Re}[T_{10}^{1\nu}]_{2p_j}^m} \right\}. \quad (6)$$

The subshell time delay, averaged over the initial m projections and summed of the final spin of the photoelectron ν , is given by the weighted sum,

$$\bar{\tau}_{2p_j} = \sum_{\nu, m} \tau_{2p_j}^{\nu m} \left| [T_{10}^{1\nu}]_{2p_j}^m \right|^2 / \sum_{\nu, m} \left| [T_{10}^{1\nu}]_{2p_j}^m \right|^2. \quad (7)$$

While the angular and spin parts of the photoionization amplitudes entering Eqs. (4-5) are fully factorized using Eqs. (1-2), the radial parts Eq. (3) need to be determined numerically. In a nonresonant case, they are obtained using the relativistic-random-phase approximation (RRPA) [27, 28] which accounts for inter-shell correlations and relativistic effects. It also has the virtue of being gauge-invariant. The RRPA equations are obtained by linearizing the time dependent Dirac-Fock coupled integro-differential equations. Major electron correlations are included in this formalism via the time-forward and time-backward ring diagrams, along with the corresponding exchange terms. In the region of autoionization resonances, the RRPA is best used in conjunction with relativistic multichannel quantum defect

theory (RMQDT) [29, 30]. The RMQDT parameters, viz., the eigenphases or the quantum defects, the dipole eigenamplitudes, and the transformation matrix from the eigenchannels to the dissociation channels, vary rather slowly and smoothly over the small energy region covering the autoionizing series. In the present method, the RMQDT parameters are calculated using the RRPA at a few energies below, within and above the resonance region. Then, RRPA equations are solved for energies just below threshold where the autoionization converges, employing open-channel boundary conditions for the bound-to-bound transitions responsible for the resonances. The RMQDT method enables the reconstruction of the entire resonance spectrum using the procedure outlined in [29] and implemented in [30]. In the present calculation we consider 7 relativistic dipole transitions: $2s_{1/2} \rightarrow np_{1/2}$, $np_{3/2}$, $2p_{1/2} \rightarrow \epsilon s_{1/2}$, $\epsilon d_{3/2}$ and $2p_{3/2} \rightarrow \epsilon s_{1/2}$, $\epsilon d_{3/2}$, $\epsilon d_{5/2}$. First two channels from $2s$ represent excitation whereas others from $2p$ indicate ionization. The present calculations are entirely *ab initio* except that we have shifted the energies to reflect the experimental Ne $2s$ binding energy, rather than the theoretical Dirac-Fock (DF) energy.

III. RESULTS AND DISCUSSION

The time delay for photoemission from the two relativistically-split subshells, $2p_{1/2}$ and $2p_{3/2}$, in the region of the $2s \rightarrow 3p$ resonance are studied separately. Since the behaviour of the time delay in these two cases is similar, we focus our attention on the simpler, the $2p_{1/2}$. Note that the angular dependence results from the only terms in the amplitudes that depend upon angle, the spherical harmonics. Since the time delay is the energy derivative of the phase, if the amplitude consists of but a single term, the delay is clearly independent of angle. However, if there is more than one term, with differing spherical harmonics in the amplitude, then there is an angular dependence because the phases of the individual terms are weighted by the differing spherical harmonics. The key features of the phase and time delay are illustrated in Fig. 1.

As expected, from the above discussion, the transition to the final state with photoelectron spin in the positive \hat{z} direction, denoted by the spin plus superscript, Eq. (4), yields phases and time delays that are angle-dependent, while the transition to the minus spin state, Eq. (5), results in an isotropic phase and time delay. More importantly, the plus phases for various angles are very significantly different from each other, leading to dramatic differences in the angular distribution of time delay seen in the upper right panel of Fig. 1. The time delay at a given photoemission angle can be positive or negative, depending upon the energy. Furthermore, at a given energy, the time delay can be positive or negative, depending upon the angle. The excursions of the time delay are very large, with positive delays up to 0.2 ps and negative

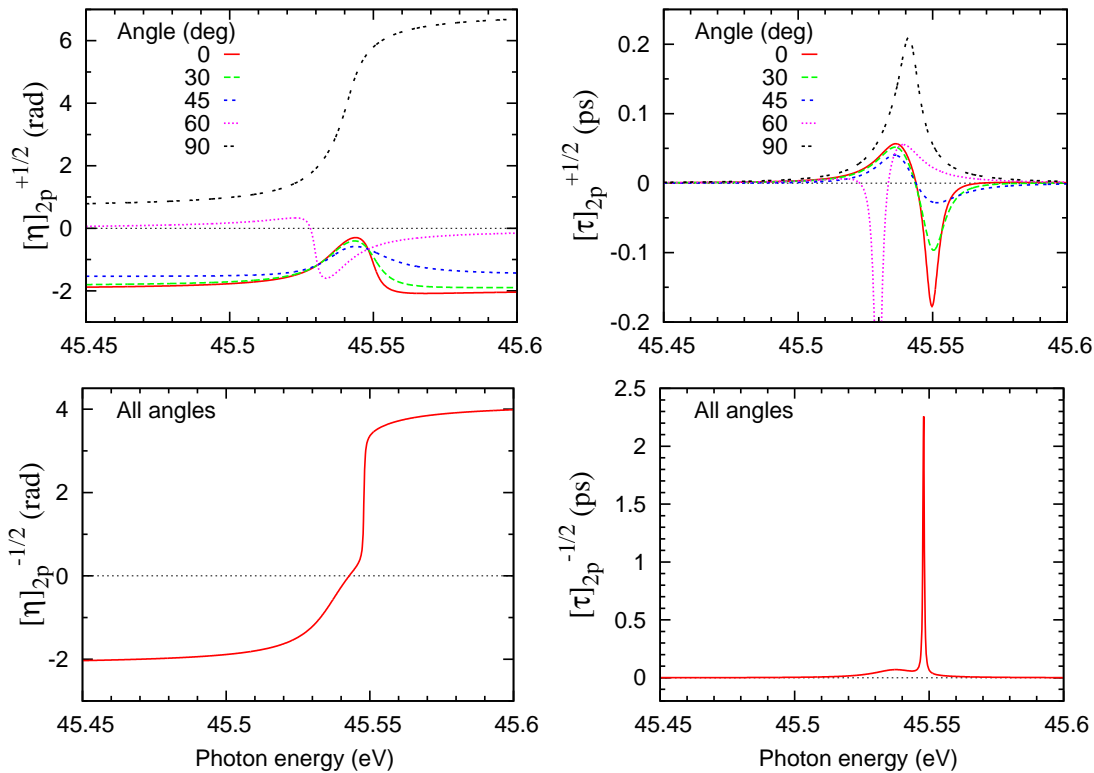


FIG. 1: (Color online) Phases in radians (left) and associated time delays in ps (right) for the Ne $2p_{1/2}$ amplitudes of Eq. (4) (top) and Eq. (5) (bottom)

delays down to -0.4 ps. This contrasts with nonresonant time delays which are at the attosecond level. Thus, the time delays in the resonance region are about five orders of magnitude larger than nonresonant delays [10–13, 16–19]; they are also considerably larger than the delays in the vicinity of a similar resonance in Ar [23].

For the spin minus state, Eq. (5), different phenomenology is evident from Fig. 1, since the phase and time delay are isotropic. However, the phase changes rather sharply, as a function of energy, leading to a time delay which maximizes at about 2 ps; in the context of attosecond time delay, this is 2,000,000 as. Since the amplitude for this transition, Eq. (5), consists of a single term, the phase and time delay are simply characteristic of the complex $2p_{1/2} \rightarrow \epsilon d_{3/2}$ matrix element. The transition to the spin plus final state, Eq. (4), is more complicated since it is a linear combination of the $2p_{1/2} \rightarrow \epsilon d_{3/2}$ and $2p_{1/2} \rightarrow \epsilon s_{1/2}$ matrix elements. Since part of the coefficient of the $2p_{1/2} \rightarrow \epsilon s_{1/2}$ matrix element is the spherical harmonic Y_{00} , which is constant and never vanishes, the $2p_{1/2} \rightarrow \epsilon s_{1/2}$ matrix element is present for all angles. Thus, even though the magnitude of the $2p_{1/2} \rightarrow \epsilon d_{3/2}$ matrix element is generally significantly larger than $2p_{1/2} \rightarrow \epsilon s_{1/2}$, the latter contributes at all angles, which makes the phase of the transition to the plus spin state, Eq. (4), rather different from the minus state, Eq. (5), especially insofar as the rapid rise of the phase is concerned. On the other hand, the coefficient of the $2p_{1/2} \rightarrow \epsilon d_{3/2}$ matrix element in Eq. (4)

contains Y_{20} which vanishes at the so-called magic angle [31], about 54° , where only the $2p_{1/2} \rightarrow \epsilon s_{1/2}$ matrix element contributes to the transition amplitude. Thus, at 60° , quite close to the magic angle, the coefficient is small and the $2p_{1/2} \rightarrow \epsilon s_{1/2}$ matrix element dominates, leading to an angular dependence of the phase and time delay for the plus transition which are different from the other angles shown in Fig. 1. It is clear, then, that spin-polarized time delay measurements of the spin plus transition at the magic angle, and the spin minus transition at any angle, would result in the experimental determination of the phases (and time delays) of the individual matrix elements. Obtaining the magnitudes and the phases of transition matrix elements is the ultimate goal of experimental physics; the magnitudes obtained from cross sections, and the phases obtained by spin-resolved measurements as explained above. And such spin-polarized measurements are essentially a reality at present [32, 33].

The situation remains of interest even if the photoelectron spin is not resolved, and the time delay is the weighted average, Eq. (7). This averaged time delay, shown for $2p_{1/2}$ in Fig. 2, shows that some of the variation of the time delay with energy and angle, seen in Fig. 1, is diminished owing to the averaging. The angular dependence is similar to the positive spin channel alone because the magnitudes of the amplitudes of Eq. (4) are generally significantly larger than Eq. (5) owing to angular momentum factors. That this is not always true is evident in the time delay at 60° , where the averaged

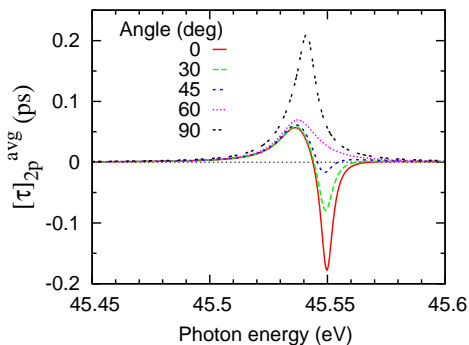


FIG. 2: (Color online) Average time delay, Eq. (7), for the photoemission from the $2p_{1/2}$ subshell of Ne in the vicinity of the $2s \rightarrow 3p$ autoionizing resonance.

results of Fig. 2, are rather different than those shown in the upper right panel of Fig. 1; the deep minimum has entirely vanished. In other words, some of the physics is lost in taking the average.

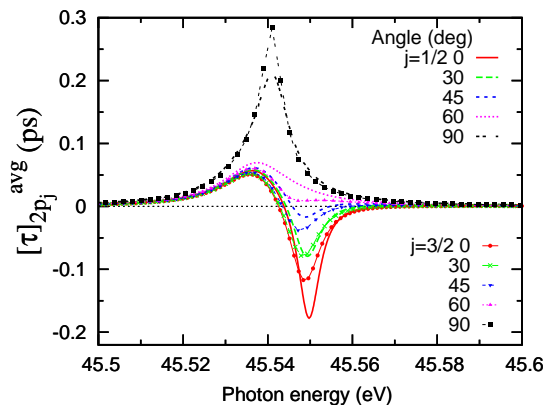


FIG. 3: (Color online) Averaged time delays for the photoemission from the $2p_{1/2}$ and $2p_{3/2}$ subshells of Ne in the vicinity of the $2s \rightarrow 3p$ autoionizing resonance.

Similar considerations apply to photoemission time delay from the $2p_{3/2}$ subshell, but the analysis is more complicated because there are four amplitudes in this case [26]. However, comparing $2p_{1/2}$ with the $2p_{3/2}$ reveals role of relativistic interactions; this comparison is shown in Fig. 3 where relativity is indeed seen to affect the results, even at such a low Z and so small an energy. From Fig. 3, near the maxima and minima at certain angles, differences of the order of 40% are in evidence. Note also that at 90° , the $2p_{3/2}$ time delay maximizes at a value significantly larger than $2p_{1/2}$, while at 0° , the maximum magnitude of the time delay (negative, in this case) is rather larger for $2p_{1/2}$. This indicates that small as they are, relativistic interactions play an important role (changes in magnitudes) and a subtle one (changes in which subshell has the larger time delay).

Finally, the average 2p time delay is considered; this

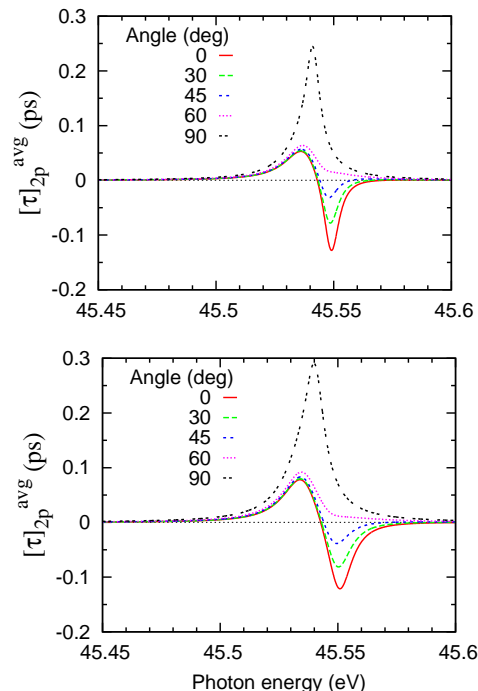


FIG. 4: (Color online) Average time delay for photoemission from the unresolved 2p subshell of Ne in the vicinity of the $2s \rightarrow 3p$ autoionizing resonance. Top: RRPA+RMQDT calculation, bottom: analytical model, Eq. (8).

is simply the average of $2p_{1/2}$ and $2p_{3/2}$ average time delays, weighted by their respective differential cross sections in the same manner as Eq. (7), and is shown on the top panel of Fig. 4. The results are very similar to the time delays depicted in Fig. 3. Of interest is that, despite an average over averages, the dramatic variation of time delay with energy and angle across the resonance remains, so that experimental investigation, even without energy resolution of the two spin-orbit-split subshells or spin-resolution of the photoelectrons, would still be quite fruitful.

This variation can be understood from a simple analytical model. We parameterize the amplitudes T_a of the strong $2p \rightarrow \epsilon d$ channel and T_b of the weak $2p \rightarrow \epsilon s$ channel near the resonance as

$$T_a = D_a \left[1 + \rho \frac{q - i}{\epsilon + i} \right], \quad T_b = D_b \left[1 - \rho \frac{q - i}{\epsilon + i} \right] \quad (8)$$

with Fano parameters $\rho^2 = 0.7$, $q = -1.6$, and $\epsilon = (\omega - \omega_0)/(\Gamma/2)$, $\omega_0 = 45.55$ eV, $\Gamma = 0.013$ eV from [34]. The nonresonant amplitudes D_a, D_b , are taken from non-relativistic RPAE calculations. For truly practical parameterizations, these amplitudes and phases can be deduced from the measurable nonresonant $2p$ photoionization cross section and angular anisotropy β parameter.

The resonant amplitudes, presented in Fig. 5, are analogous to amplitudes for the $3s \rightarrow 4p$ autoionizing resonance in Ar shown in Fig. 7 of [23]. Outside the res-

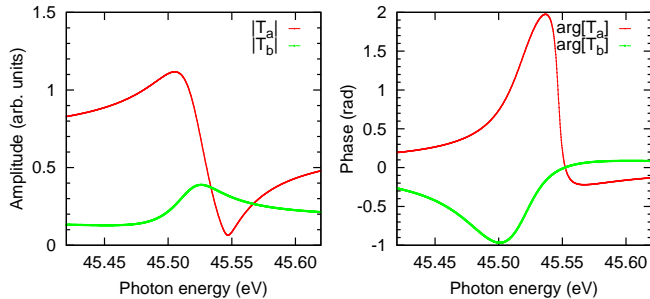


FIG. 5: (Color online) Moduli (left) and phases (right) of the resonant amplitudes T_a, T_b Eq. (8) .

onance, the strong amplitude is dominant and the orbital d -character determines the angular symmetry of the ionized photoelectron wave packet. Because this orbital character is unique, there is no angular dependence of the time delay. Near the resonance, the strong amplitude drops rapidly in magnitude and the competition with the nominally weak amplitude becomes intense. This explains the angular dependence of the time delay near the resonance. The strong and weak amplitudes vary near the resonance out of phase. Hence the time delay makes positive and negative oscillations as the energy increases. Beyond the magic angle of 54° , the spherical harmonic supporting the strong amplitude changes its sign and the energy oscillation of the two amplitudes becomes in phase, making the time delay always positive.

IV. CONCLUSION

In summary, the Wigner time delay, in the vicinity of a Fano resonance, exhibits dramatic variation with energy and angle, with the time delay even being of opposite signs at different angles at the same energy. Relativistic interactions were found to induce significant effects, even at such low Z , suggesting that time-delay chronoscopy might be a useful tool in probing relativistic interactions. And it was shown how the recently-developed spin-polarized time delay spectroscopy could be used to determine the phases of individual transition matrix elements. Note that there is nothing special about the particular resonance studied so that the phenomenology uncovered should be qualitatively similar for other resonances and other systems. Finally, we note that the effect of the probing laser field used to measure WTD goes beyond the scope of this investigation. For a resonant transition, this effect has been considered in [23, 35, 36]. We believe that the present study would stimulate further interest for experimental explorations.

ACKNOWLEDGEMENT

This work was supported by the Chemical Sciences, Geosciences, and Biosciences Division, Office of Basic Energy Sciences, Office of Science, US Department of Energy.

-
- [1] M. F. Limonov *et al*, Nat. Photon. **11**, 543 (2017)
 - [2] Chia Wei Hsu *et al*, Nat. Rev. Mat. **1**, 16048 (2016)
 - [3] C. Ott *et al*, Nature **516**, 374 (2014)
 - [4] E. P. Wigner, Phys. Rev. **98**, 145 (1955).
 - [5] L. E. Eisenbud, Ph. D. thesis, Princeton Univ. (1948).
 - [6] F. T. Smith, Phys. Rev. **118**, 349 (1960).
 - [7] M. Schultze *et al*, Science **328**, 1658 (2010).
 - [8] K. Klünder *et al*, Phys. Rev. Lett. **106**, 143002 (2011).
 - [9] R. Pazourek *et al*, Rev. Mod. Phys. **87**, 765 (2015).
 - [10] A. S. Kheifets *et al*, Phys. Rev. A **92**, 063422 (2015).
 - [11] P. Hockett *et al*, J. Phys. B **49**, 095602 (2016).
 - [12] M. Huppert *et al*, Phys. Rev. Lett. **117**, 093001 (2016).
 - [13] S. Heuser *et al*, Phys. Rev. A **94**, 063409 (2016).
 - [14] V. Gruson *et al*, Science **354**, 734 (2016).
 - [15] M. Isinger *et al*, Science **358**, 893 (2017).
 - [16] D. A. Keating *et al* J. Phys. B **50**, 175001 (2017).
 - [17] L. Gallmann *et al*, Struct. Dynam. **4**, 061502 (2017).
 - [18] C. A Nicolaidis, Appl. Sci. **8**, 533 (2018).
 - [19] D. A. Keating *et al* Phys. Rev. A **98**, 013420 (2018).
 - [20] M. Sabbar *et al*, Phys. Rev. Lett. **115**, 133001 (2015).
 - [21] M. Kotur *et al*, Nat. Comm. **7**, 10566 (2016).
 - [22] P. C. Deshmukh *et al*, J. Phys. B **51**, 065008 (2018).
 - [23] C. Cirelli *et al*, Nat. Comm. **9**, 955 (2018).
 - [24] J. Vos *et al*, Science **360**, 1326 (2018).
 - [25] M. Nrisimhamurthy *et al*, Phys. Rev A **91**, 013404 (2015).
 - [26] A. Kheifets *et al*, Phys. Rev. A **94**, 013423 (2016).
 - [27] W. R. Johnson and C. D. Lin, Phys. Rev. A **20**, 964 (1979).
 - [28] W. R. Johnson and K. T. Cheng, Phys. Rev. Lett. **40**, 1167 (1978).
 - [29] C. M. Lee and W. R. Johnson, Phys. Rev. A **22**, 979 (1980).
 - [30] W. R. Johnson *et al*, Phys. Rev. A **22**, 989 (1980).
 - [31] S. T. Manson and A. F. Starace, Rev. Mod. Phys. **54**, 389 (1982) and references therein.
 - [32] M. Fanciulli *et al*, Phys. Rev. Lett. **118**, 067402 (2017).
 - [33] M. Fanciulli and J. H. Dil, arXiv:1806.05895
 - [34] K. Codling, R. P. Madden, and D. L. Ederer, Phys. Rev. **155**, 26 (1967).
 - [35] A. Jiménez-Galán, L. Argenti L and F. Martín Phys. Rev. Lett. **113**, 263001 (2014)
 - [36] A. Jiménez-Galán, F. Martín and L. Argenti Phys. Rev. A **93**, 023429 (2016)